Microchimica Acta (2019) 186: 373
https://doi.org/10.1007/s00604-019-3428-3

ORIGINAL PAPER

Fluorescent methionine-capped gold nanoclusters for ultra-sensitive determination of copper(II) and cobalt(II), and their use in a test strip

Fuming Sang[1] · Xue Zhang[1] · Fengyi Shen[1]

Received: 11 December 2018 / Accepted: 10 April 2019 / Published online: 23 May 2019

Abstract

A fluorometric assay was constructed for supersensitive determination of Cu^{2+} and Co^{2+} based on their quenching effect on the orange fluorescence of methionine-capped gold nanoclusters (Met-AuNCs). A simple one-step method was developed for the preparation of the Met-AuNCs, employing L-methionine as both a reducing and protecting reagent. Within 10 min, water soluble Met-AuNCs were obtained with an average size of 2.4 nm. Under photoexcitation at 370 nm, the Met-AuNCs possess a maximum emission at 580 nm and a quantum yield of 2.3%. The response is fast (1 min), and the selectivity for Cu^{2+} and Co^{2+} is high over other metal ions. The detection limits for Cu^{2+} and Co^{2+} are around 47 and 420 pM, respectively. The effects were used to design a test paper for visual detection of Cu^{2+} and Co^{2+}. Using this test paper, 1 μM of Cu^{2+}/Co^{2+} can be detect under the UV lamp (365 nm excitation). It is perceived to be a promising tool for the rapid on-site determination of Cu^{2+} and Co^{2+} in real water samples.

Keywords Methionine · Gold nanoclusters · Fluorescence quenching · Cu^{2+} · Co^{2+}

Introduction

The ions Cu^{2+} and Co^{2+} are essential micronutrients that play important roles in biosynthesis and metabolism [1, 2]. However, Cu^{2+} and Co^{2+} ions can be harmful to health at high levels [3, 4]. Moreover, Cu^{2+} and Co^{2+} result in metal contaminations due to their wide industrial applications. Accordingly, facile and sensitive assays for detection of Cu^{2+} and Co^{2+} are needed, especially for biomedical and environmental fields.

Various analytical methods mainly consisting of solid phase extraction (SPE) [1], inductively coupled plasma mass spectroscopy (ICP-MS) [5], inductively coupled plasma optical emission spectrometry (ICP-OES) [6], flame atomic absorption spectrometry (FAAS) [7, 8], and high performance liquid chromatography coupled with inductively coupled plasma mass spectrometry (HPLC-ICP-MS) [9] have been used for the detection of Cu^{2+} and Co^{2+}. However, these methods often suffer from relatively high cost, time-consuming analysis or pretreatment procedures which restrict them from being applied in the simple, rapid and on-site determination [8, 10–13].Accordingly, it is still a great challenge to exploit a simple, low cost, portable and sensitive sensing assay for real-time detection of Cu^{2+} and Co^{2+} ions.

Gold nanoclusters (AuNCs) are attracting great attentions owing to their low toxicity, biocompatibility, facile synthesis, high fluorescence emission, large stokes shift [14]. Many "green" ways have proposed to prepare AuNCs by directly reducing $HAuCl_4$ with reducing-cum-stabilizing reagent [15]. For example, some macromolecules protein [16], dendrimer [17] and natural polymer [18–20] have been employed as reducing and protecting reagents to synthesise highly fluorescent AuNCs. In addition, some small biomolecules, such as glutathione, amino acids (tyrosine, L-proline and histidine) have been used for preparing AuNCs through a simple one-pot reaction [21–24]. However, most of them need tedious

---

Electronic supplementary material The online version of this article (https://doi.org/10.1007/s00604-019-3428-3) contains supplementary material, which is available to authorized users.

✉ Fuming Sang
sangfuming@hitwh.edu.cn

[1] School of Marine Science and Technology, Harbin Institute of Technology, Weihai 264209, People's Republic of China

procedures, costly ligands and a very long reaction time from several hours to days, which restrict their wide applications [25]. Consequently, it is very desirable to develop a facile and rapid method for the preparation of fluorescent AuNCs.

Herein, we demonstrate a simple and fast synthetic approach of AuNCs using methionine as both a reducing and protecting reagent. Within 10 min, the Met-AuNCs with excitation/emission peaks at 370/580 nm were synthesized. Moreover, the Met-AuNCs were used as fluorescent probe to detect Cu^{2+} and Co^{2+} with a low detection limit of 47 pM and 0.42 nM respectively, which were more sensitive than the previous analytical methods. To illustrate the practicality of the assay, it was further applied to the determination of Cu^{2+} and Co^{2+} in environmental water samples. More importantly, we transferred such a new assay to test paper, and good results were attained within 1 min with the minimum visual detection concentration down to 1 μM for Cu^{2+} and Co^{2+} by the bare eyes.

Experimental section

Materials and reagents

Tetrachloroauric acid ($HAuCl_4$), L-methionine, NaOH were from Sinopharm Chemical Reagent Co. Ltd. (Shanghai, China, http://www.reagent.com.cn/). Ethylenediaminetetraacetic acid (EDTA), $CoCl_2·6H_2O$ and $CuSO_4·5H_2O$ were purchased from Aladdin Reagent Company (Shanghai, China, http://aladdin.company.lookchem.cn/). The other inorganic salts of cations (Co^{2+}, Cu^{2+}, Ni^{2+}, Fe^{3+}, Mn^{2+}, Al^{3+}, Ca^{2+}, Zn^{2+}, Ag^{+}, Ba^{2+}, Hg^{2+}, Cd^{2+}, Na^{+}, K^{+}, Mg^{2+}, Cr^{3+}, Fe^{2+}, Pb^{2+}, Pt^{2+}) and the filter papers were obtained from Sangon Biotechnology Company, Ltd. (Shanghai, China, http://www.sangon.com/). All the solutions used in the experiments were prepared using deionized water (18 MΩ·cm).

Instrumentations

The UV-vis absorbance spectra were measured on a TU1810 UV-vis spectrophotometer (Beijing Purkinje General Instrument, Beijing, China). The fluorescent spectra were measured with a fluorescence spectrometer F-2700 (Hitachi, Tokyo, Japan). Transmission electron microscopy (TEM) images were recorded using a JEOL JEM2010 microscope at 200 kV. Dynamic light scattering (DLS) data was collected on a Zetasizer Nano ZS90 instrumentation (Malvern Instruments Ltd., UK). The Fourier transform infrared spectroscopies (FT-IR) were measured using a Perkin Elmer Paragon 1000 FT-IR spectrometer (Waltham, MA, USA).

Synthesis of methionine-capped gold nanoclusters (Met-AuNCs)

All glass instruments for experiment were immersed into aqua regia (HCl/HNO_3 3:1 *v*/v), flushed completely with deionized water, and then dried before use. Initially, 1 mL of methionine solution (0.16 M) was mixed with 200 μL of $HAuCl_4$ solution (10 mg/mL). Then, 100 μL of NaOH solution (0.04 M) was rapidly added into the foregoing mixed solution and mixed for 1 min to obtain an homogeneous solution. After 10 min of incubation at 75 °C, the solution was taken out from the heater followed by slowly cooling to ambient temperature. After centrifugation at 10,000 rpm for 10 min to discard large particles, the Met-AuNCs were preserved at 4 °C in the dark until subsequent application.

Quantum yield (QY) of Met-AuNCs

The QY of the Met-AuNCs was measured using Rhodamine 6G in ethanol as the standard. The QY was obtained with the following equation [26]:

$$\phi_X = \phi_{ST}\left(\frac{Grad_X}{Grad_{ST}}\right)\left[\frac{n_X}{n_{ST}}\right]^2$$

where the subscripts ST and X represent reference solution and Met-AuNCs, respectively, Φ is the luminescence QY value, *Grad* is the gradient from the plot of integrated emission intensity versus the corresponding absorption value, and n is the refractive index of the water or ethanol.

Fluorometric detection of Cu^{2+} and Co^{2+}

100 μL of Met-AuNCs was added into 890 μL of phosphate buffered solution buffer (10 mM, pH = 8). Metal ions (Cu^{2+} and Co^{2+}) with different concentrations (10 μL, ranging from 0 to 1 mM) were then added and mixed thoroughly. After 1 min incubation at ambient temperature, the corresponding fluorescence quenching spectra were measured (λ_{exc} /λ_{em} = 370/580 nm); slit widths for both the excitation and emission were set at 5 nm. The interfering experiments of the other metal ions were studied individually with Met-AuNC solution under the same conditions.

Analysis of environmental water samples

Tap water, lake water, sea water and waste water samples were obtained from our laboratory, the Sun and Moon Lake on the campus of Harbin Institute of Technology (Weihai) and golden beach of Weihai. All the samples were pretreated by centrifugation (10,000 rpm, 10 min) and filtered through 0.45 μM filters to remove any suspended impurities. And then, a series of samples were obtained by spiking standard solution

(500 μL) with various concentrations of Cu^{2+}/Co^{2+} (0 to 200 μM) in 20 mM phosphate buffered solution buffer (pH = 8) into the tap water, lake water and sea water (400 μL), respectively. Then, the Met-AuNCs (100 μL) were added into the above resulting solutions. After 1 min incubation at room temperature, the corresponding fluorescence quenching spectra were attained ($\lambda_{ex}/\lambda_{em} = 370/580$ nm).

Preparation of fluorescent test papers and sensing applications

In order to prepare AuNCs-based test papers, filter papers were cut into small pieces with a diameter of 1 cm prior to use. Small pieces of papers were immersed into the Met-AuNC aqueous solution for 2 h and dried at 40 °C for 40 min. The test papers were submerged separately in 1 mL of the different ions solutions with various concentrations (100 nM to 1 mM) for 1 min at ambient temperature and dried at 40 °C for 10 min. The changes in the fluorescent test papers were observed under a UV light ($\lambda_{ex} = 365$ nm). Tweezers were used in the aforementioned process.

Results and discussion

The synthesis and characterization of Met-AuNCs

In this work, Met-AuNCs were synthesized by a rapid one-pot synthesis via the reduction of gold ions with methionine as both as both reductant and stabilizer (as illustrated in Scheme 1). Synthesis conditions including methionine concentration, NaOH concentration, reaction time and temperature were optimized. As illustrated in Fig. S1a, the optimal concentration of methionine was 0.16 M, in which the strongest fluorescence of Met-AuNCs was obtained. The influence of the NaOH concentration on the Met-AuNCs fluorescence is illustrated in Fig. S1b. It can be seen that the appropriate concentration was 40 mM which gave the highest fluorescence intensity. Figure S1c demonstrated that the fluorescence intensity was also influenced by the reaction temperature. The fluorescence intensity increased with increasing temperature (35 to 75 °C). The strongest fluorescence was obtained at 75 °C. However, it is reduced at higher temperature (85 and 90 °C), which may be that high temperature easily led to the nanocluster aggregation [14]. Consequently, 75 °C was used in the all experiments. Moreover, it was clear that the synthesis process merely needed 10 min (for chemical reaction only) under the optimal conditions (Fig. S1d). As the increasing of reaction time, the fluorescent intensity of AuNCs started to decrease, which may be due to the beginning of clusters degradation. Accordingly, 10 min was adopted as the optimum reaction time. In a word, this proposed synthesis process was a rapid, facile and green approach.

Met-AuNC solution showed pale yellow under daylight and orange red under a UV lamp (365 nm) (inset c and f of Fig. 1a, respectively), whereas neither pure methionine nor $HAuCl_4$ emitted fluorescence in the same conditions, indicating that the high fluorescence stems from the luminescence of

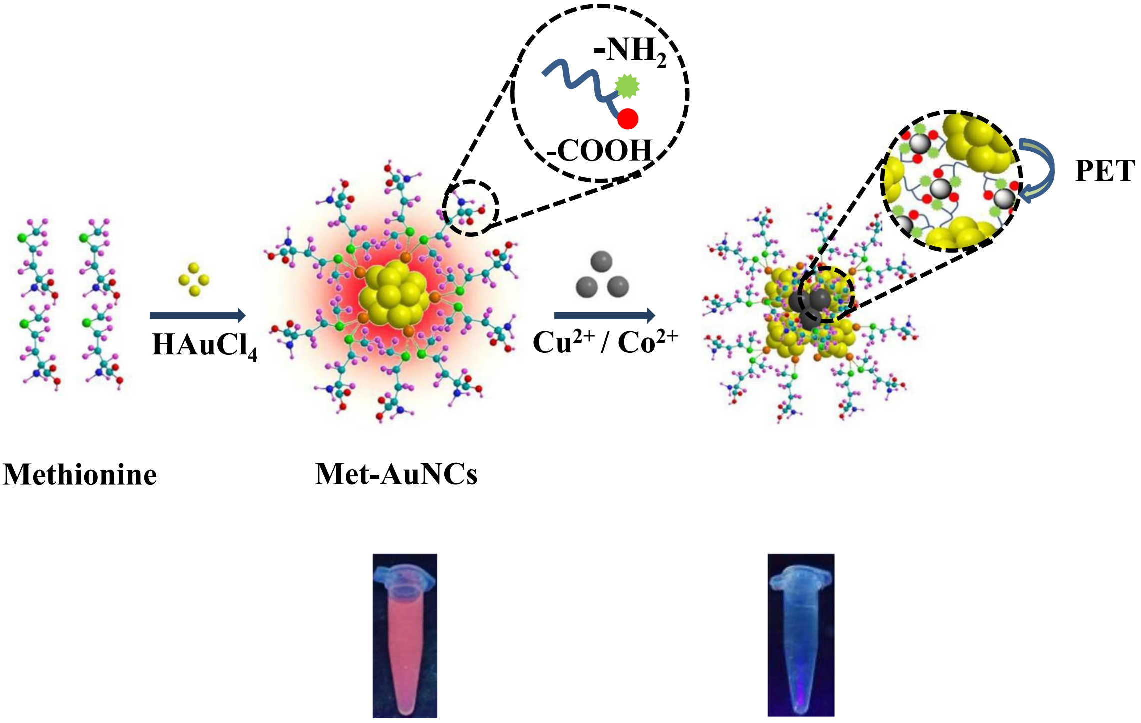

Scheme 1 Scheme of the formation of Met-AuNCs and used as a fluorescent probe for the detection of Cu^{2+} and Co^{2+}

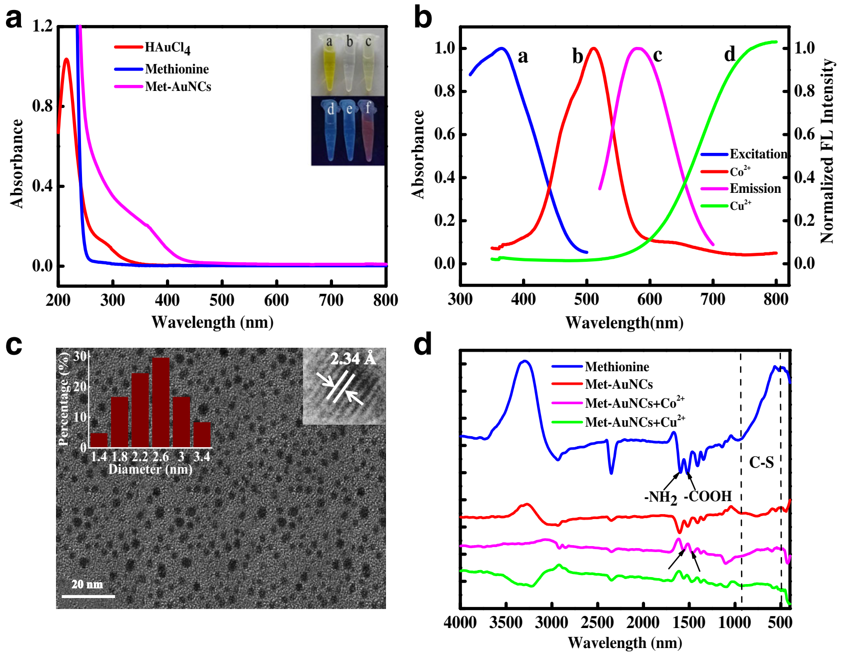

Fig. 1 **a**: UV-vis absorption spectra of the aqueous $HAuCl_4$, methionine and Met-AuNCs. Inset: photographs of the $HAuCl_4$ under room light (a) and UV light ($\lambda_{ex} = 365$ nm) (d), methionine under room light (b) and UV light ($\lambda_{ex} = 365$ nm) (e), and Met-AuNCs under room light (c) and UV light ($\lambda_{ex} = 365$ nm) (f); **b**: Flourescence exitation (a) and emission spectra (c) of Met-AuNCs at room temperature, UV-vis absorption spectrum of Co^{2+} (b) and Cu^{2+} (d); **c**: TEM image of Met-AuNCs and HR-TEM image of a single AuNC (inset); **d**: FT-IR spectra of methionine and Met-AuNCs in the absence and presence of Co^{2+} and Cu^{2+}

Met-AuNCs. Figure 1a demonstrates the absorption spectrum of Met-AuNCs. The outstanding surface plasmon absorption peak of large AuNPs (around 520 nm) missed which demonstrated that the most Met-AuNCs sizes were less than 2.5 nm. Instead, an obvious absorption band at 360 nm was observed. In contrast, no absorption peaks at 360 nm were obtained in the pure methionine and $HAuCl_4$ solutions. As shown in Fig. 1b, the Met-AuNCs exhibited an excitation peak centered at 370 nm and an emission peak centered at 580 nm. Met-AuNCs are superior to the organic fluorophores, which have a large stokes shift of 210 nm, can refrain from the mutual interference between the excitation and emission signals. Moreover, the emission spectra peaks of AuNCs remained unchanged at different excitation wavelengths (350–490 nm Fig. S2), demonstrating that the fluorescent property of AuNCs was attributed to vibrational relaxation but not scattering effects [27]. As shown in Fig. S3, the QY of luminescent Met-AuNC solution was measured at 2.3% using Rhodamine 6G as the reference. The Met-AuNCs illustrate good storage and high salt stability (Fig. S4a). Figure S4b shows that the fluorescence intensity has no obvious change after one month storage at 4 °C, indicating the good storage stability. TEM image illustrates that AuNCs display spherical shape and well dispersed with the mean size of 2.4 nm (Fig. 1c). The HR-TEM image (inset of Fig. 1c) demonstrated a single AuNC with a lattice fringe of 0.234 nm, corresponding to the (111) lattice plane of AuNCs, and confirmed the crystal structure of the metallic Au [28]. As shown in Fig. S5, the Met-AuNCs presented four characteristic X-ray diffraction (XRD) peaks at 38.1°, 44.2°, 64.6° and 77.6°. On the basis of the Bragg equation [29], the peak located at 38.1° corresponding to the (111) planes of crystalline gold shows 2.34 Å lattice spacing, which is consistent with the TEM result. FT-IR spectra (Fig. 1d) revealed that no apparent shift or disappearance of ν_{as} NH_3^+ (1597 cm^{-1}) and ν_{as} COO^- (1520 cm^{-1}) of the methionine was observed in Met-AuNCs with the exception of a suppression of the -C-S stretching vibration (600–800 cm^{-1}). Therefore, we deduced that S-atom but not -NH_2 and -COOH groups of the methionine participated in the bonds formation in Met-AuNCs.

Optimization of the conditions

The following parameters were optimized: (a) amount of Met-AuNCs; (b) sample pH value; (c) incubation time. Respective data and Figures are given in the Electronic Supporting Material. The following experimental conditions were found to give best results: (a) optimal amount of Met-AuNCs: 100 µL; (b) best sample pH value: 8; (c) optimal incubation time: 1 min.

Highly sensitive detection of Cu^{2+} and Co^{2+}

To evaluate Met-AuNCs as a fluorescent probe for the assays of both Cu^{2+} and Co^{2+}, the fluorescence changes were measured after the titration of different concentrations of Cu^{2+} and Co^{2+} (0 to 100 µM) under the optimum reaction conditions. As illustrated in Fig. 2a, the fluorescence emission intensity of Met-AuNCs at 580 nm gradually reduced as the Cu^{2+} concentration increased. There was a good linear dependence between the quenching fluorescence intensity (I_0/I, I and I_0 represented the fluorescence intensity at 580 nm with and without Cu^{2+}, respectively) and Cu^{2+} concentration with $R^2 = 0.9976$ over a wide range of 0.0001–6 µM (Fig. 2b). Particularly, with

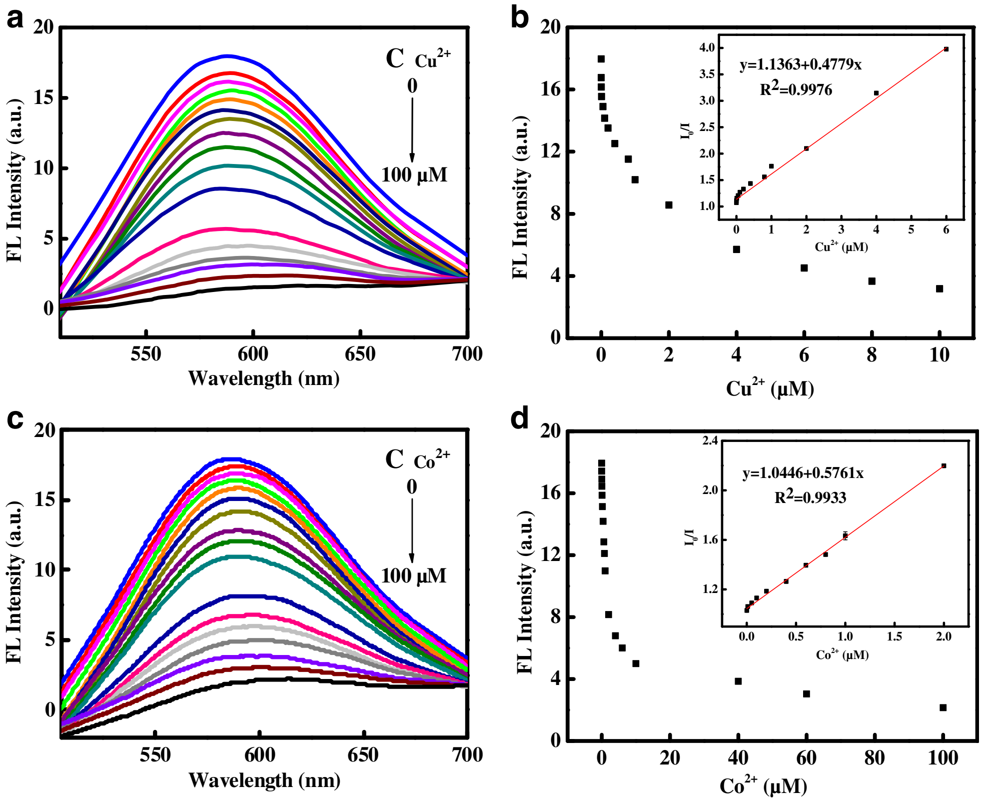

Fig. 2 **a:** Fluorescence spectra of Met-AuNCs after the addition of Cu^{2+} at various concentrations within 0–100 μM; **b**: the fluorescent response (I_0/I) of Met-AuNCs to Cu^{2+}. The inset of part B shows the linear calibration plot for Cu^{2+} detection within 0–6 μM; **c:** fluorescence spectra of Met-AuNCs with the addition of Co^{2+} at various concentrations within 0–100 μM; **d**: the fluorescent response (I_0/I) of Met-AuNCs to Co^{2+}. The inset of part B shows the linear calibration plot for Co^{2+} detection within 0–2 μM. Error bars were obtained from three experiments

the increasing of the Cu^{2+} concentration, an obvious red shift phenomenon was observed. Similarly, the fluorescence intensities at 580 nm decreased as the Co^{2+} concentration augmented, and a linear calibration graph with a correlation coefficient of $R^2 = 0.9933$ was attained between the intensity ratios (I_0/I, I and I_0 represented the fluorescence intensities at 580 nm with and without Cu^{2+}, respectively) and Co^{2+} concentration within 0.001–2 μM (Fig. 2c and d). For the sake of assessing the sensitivity of the assay, 3α/slope was used to calculate the detection limit of the sensor [30], where α referred to the standard deviation of the instrument and slope was obtained from the linear calibration plot. The limits of detection (LOD) for Cu^{2+} and Co^{2+} ions were 0.047 and 0.42 nM, respectively. More importantly, the LODs are much lower and compare favorably with the previous reported analytical assays, which can be seen in Table S1 and 2. Moreover, the LODs are much lower than the limit of detection requirements of Cu^{2+} and Co^{2+} in drinking water (31.5 and 1.7 μM, respectively).

Selectivity of the Met-AuNCs for the detection of Cu^{2+} and Co^{2+}

To evaluate whether the developed fluorescent assay was specific for $Cu^{2+}$and Co^{2+} ions, the fluorescence responses of the sensing system were measured with various metal cations and anions (Co^{2+}, Cu^{2+}, Ni^{2+}, Fe^{3+}, Mn^{2+}, Al^{3+}, Ca^{2+}, Zn^{2+}, Ag^+, Ba^{2+}, Hg^{2+}, Cd^{2+}, Na^+, K^+, Mg^{2+}, Cr^{3+}, Fe^{2+}, Pb^{2+}, Pt^{2+}). As shown in Fig. 3a, only Cu^{2+} and Co^{2+} triggered the obvious quenching of the Met-AuNCs fluorescence, and the other cations showed minor interferences on the fluorescence intensity ratio of Met-AuNCs. Photograph of Met-AuNC solution in the presence of different metal ions were observed under a UV lamp (365 nm) and are displayed in Fig. S7a. It was obviously seen that the orange red fluorescence vanished only in the presence of Cu^{2+} and Co^{2+}, while the others still remained the orange red fluorescence. Based on the above-mentioned results, we further attempted to prepare Met-AuNCs based fluorescent test paper to facilitate the portable sensing application (the detailed preparation method was presented in the Experimental Section). As demonstrated in Fig. 3b, the fluorescence color of the blank test paper was orange red under UV lamp (365 nm). However, the orange red fluorescence disappeared totally with the addition of Cu^{2+} and Co^{2+}, while the other ions samples almostly remained the orange red fluorescence color as the blank test paper. Therefore, these results illustrated that the Met-AuNCs were specific and had a prominent selectivity for Cu^{2+} and Co^{2+}.

To further confirm the selectivity of the Met-AuNCs, interference studies using different ions along with Cu^{2+} and Co^{2+} were performed. As shown in Fig. S7b, it was obvious that Met-AuNCs showed highly selective fluorescence quenching towards Cu^{2+} and Co^{2+} ions in a mixture of different ions. Moreover, tartaric acid was chosen as masking agent to distinguish Cu^{2+} and Co^{2+}. As shown in Fig. S8, the fluorescence

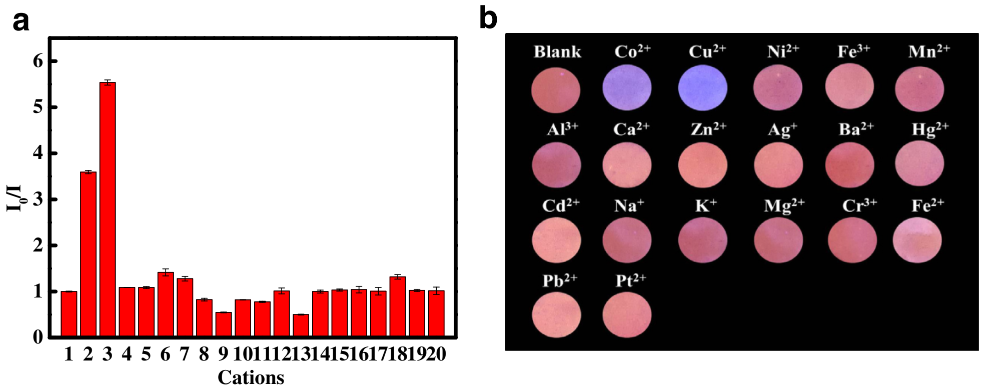

Fig. 3 Selectivity of the Met-AuNCs based sensing system to various metal ions (Co^{2+} and Cu^{2+} 10 μM, other ions 30 μM). **a**: Samples marked with 1–20 corresponding to blank, Co^{2+}, Cu^{2+}, Ni^{2+}, Fe^{3+}, Mn^{2+}, Al^{3+}, Ca^{2+}, Zn^{2+}, Ag^{+}, Ba^{2+}, Hg^{2+}, Cd^{2+}, Na^{+}, K^{+}, Mg^{2+}, Cr^{3+}, Fe^{2+}, Pb^{2+}, Pt^{2+}, respectively; **b**: Photographic images of Met-AuNCs based fluorescent test papers exposed to various ions (10 μM)

of the Met-AuNCs quenched by Co^{2+} was recovered, whereas the analysis of Cu^{2+} is almost unaffected in the presence of tartaric acid ligand. Accordingly, these results authenticated that the other metal ions did not influence the detection of Cu^{2+} and Co^{2+}.

Mechanisms of Met-AuNCs for the detection of Cu^{2+} and Co^{2+}

Generally, fluorescence quenching mechanisms can include Förster resonance energy transfer (FRET), inner filter effect (IFE), static quenching, dynamic quenching and photoinduced electron transfer (PET) and aggregation induced quenching [31]. As shown in Fig. 1b, there were no significant overlaps between the absorption spectra of Cu^{2+}/Co^{2+} and the excitation /emission spectra of Met-AuNCs. Thus, the quenching mechanism was neither IFE nor FRET [32].

The quenching mechanisms can be usually categorized into dynamic and static quenching. Dynamic quenching involves the collision of between excited fluorophore and quenching substance, while static quenching occurs when the complex is formed between the ground state fluorescence molecule and the quencher [31, 33]. In order to explain the quenching mechanism in detail, we calculate the quenching equation on the basis of the modified Stern-Volmer equation [2]

$$I_0/I = (1 + Kd[Q])\cdot(1 + Ks[Q]) = 1 + (Kd + Ks)[Q] + KdKs[Q]^2,$$

where I_0 and I represent the fluorescence intensities of the Met-AuNCs in the absence and in the presence of Cu^{2+}/Co^{2+}, [Q] represents the concentration of the Cu^{2+}/Co^{2+} in aqueous solution, K_d is the dynamic quenching constant, and K_s is the static quenching constant. As illustrated in Fig. 2b and d, SV plot is curved, suggesting that the quenching process in the present work was both static and dynamic quenching.

To further insight into the quenching process, the effect of temperature was used to directly distinguish the static and dynamic quenching [34]. As shown in Fig. S9a and b, the quenching efficiency of Cu^{2+} and Co^{2+} gradually decreased with the increasing of the temperature, suggesting that the static quenching happened. Moreover, the obvious red shift and absorbance enhancement were observed upon the addition of various amounts of Cu^{2+} and Co^{2+} (Fig. S10a and b). The obvious changes of the absorption spectra should be attributed to the combination of Cu^{2+}/Co^{2+} ions with Met-AuNCs to their complex Met-AuNCs-Cu^{2+}/Co^{2+}. The TEM images of Met-AuNCs in the presence of Cu^{2+} and Co^{2+} ions (Fig. S11a and b) provided an obvious evidence of aggregation In addition, the zeta potential of Met-AuNCs raised from −36.7 mV to −26.6 mV and − 28.2 mV after the addition of Cu^{2+} and Co^{2+}, respectively. Therefore, the above results confirme the interaction between Cu^{2+}/Co^{2+} and Met-AuNCs.

To explore whether the fluorescence quenching of Met-AuNCs was attributed to the interaction complexation of Cu^{2+}/Co^{2+} with methionine or the high-affinity metallophilic interaction, the fluorescence recovery experiments were conducted. EDTA was chosen as a chelator with the stability

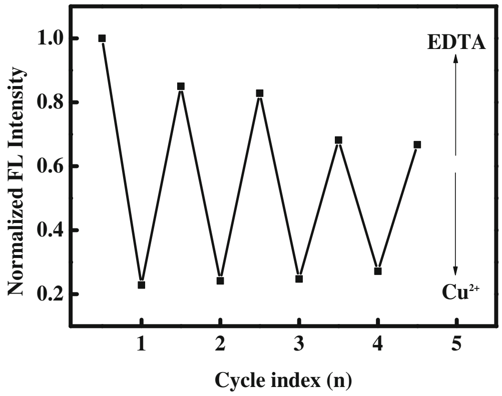

Fig. 4 Reversible investigation of the Met-AuNCs for Cu^{2+} with the addition of EDTA. 8 μM Cu^{2+} and 8.8 μM EDTA were used

Table 1 Detection of Cu^{2+} and Co^{2+} in real water samples (tap, lake and sea water) spiked with vavious concentrations of Cu^{2+} and Co^{2+} by the developed assay

Sample	Ions	Spiked (μM)	ICP (μM)	found (μM)	Recovery (%)	RSD (%) ($n = 3$)
Drinking water	Cu^{2+}	1.0	1.06	1.18 ± 0.104	118	8.81
		0.4	0.42	0.43 ± 0.023	109	5.34
Sea water	Co^{2+}	1.0	1.06	1.01 ± 0.053	101	5.25
		0.4	0.39	0.43 ± 0.021	108	4.88
Lake water	Cu^{2+}	1.0	1.04	0.99 ± 0.050	99	5.05
		0.4	0.41	0.42 ± 0.016	107	3.80
	Co^{2+}	1.0	0.98	0.97 ± 0.054	97	5.56
		0.4	0.38	0.43 ± 0.025	108	5.81
Waste water	Cu^{2+}	1.0	1.15	1.19 ± 0.110	119	9.24
		0.4	0.38	0.48 ± 0.045	120	9.37
	Co^{2+}	1.0	1.07	0.99 ± 0.050	99	5.05
		0.4	0.40	0.42 ± 0.032	105	7.62

constants (log K) of 18.7 for Cu^{2+} and 16.31 for Co^{2+}. Figure 4 showed that the fluorescence intensity of Met-AuNCs upon the addition of Cu^{2+} was recovered after introduction of an excessive dosage of EDTA. Moreover, this reversible cycle is repeated 4 times, demonstrating that the Met-AuNCs based assay is repeatable. Similar with Cu^{2+}, fluorescence intensity was attained after removing Co^{2+} by EDTA (Fig. S12). The recovery experiments demonstrated that the interaction between Cu^{2+}/Co^{2+} ions and Met-AuNCs was actually by the means of interaction complexation. Moreover, the FT-IR was used to verify the coordination between Cu^{2+} and Co^{2+} with Met-AuNCs (Fig. 1d). In the FT-IR spectra, the peak at 1597 cm^{-1} for NH_3^+ band and 1520 cm^{-1} for -COO^- band in Met-AuNCs shifted to 1560 and 1460 cm^{-1}, respectively.

However, although lots of metal ions can bind to methionine, they can not quench the fluorescence of Met-AuNCs. Accordingly, PET process should also take place, the Cyclic Voltammetry (CV) results (Fig. S13) underpin the PET process between Met-AuNCs and Cu^{2+}/Co^{2+}. As shown in Fig. S14, the energy gap between HOMO of donor and acceptor force photoinduced electron transfer. More importantly, all the above-mentioned analyses further authenticated that the quenching mechanism was both static and dynamic quenching.

Real sample analysis

For the sake of evaluating the feasibility of the sensing platform in practical application, ICP and the Met-AuNCs probe were further applied to detect Cu^{2+} and Co^{2+} amounts in real water samples. Different concentrations of Cu^{2+} and Co^{2+} were spiked into tap water, lake water, sea water and waste water samples. As listed in Table 1, satisfactory recoveries of Cu^{2+} and Co^{2+} are obtained varying from 99% to 120%, 97% to 108%, respectively, with the relative standard deviations (RSDs) changing from 3.80% to 9.37%. The results confirmed the high accuracy and good precision of the Met-AuNCs based assay in real samples.

Fluorescence test paper for the detection of Cu^{2+} and Co^{2+}

Aforementioned results prove that the Met-AuNCs detect Cu^{2+} and Co^{2+} from the other ions simultaneously with high

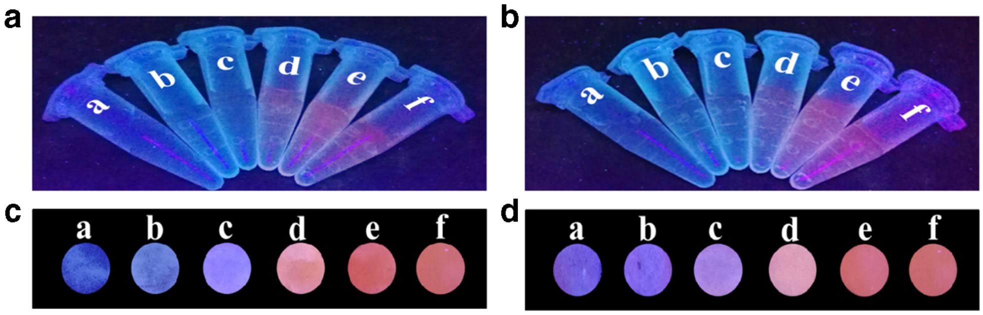

Fig. 5 Photographs images of Met-AuNCs solution in the presence of different concentrations of (**a**) Cu^{2+} and (**b**) Co^{2+}; Photographs images of Met-AuNCs based fluorescent test papers in the presence of different concentrations of (**c**) Cu^{2+} and (**d**) Co^{2+}. a-f: 1000 μM, 100 μM, 10 μM, 1 μM, 0.1 μM, 0 μM, respectively

sensitivity and specificity, having potential as a fluorescent probe. More interestingly, the fluorescence of Met-AuNC solution absolutely disappeared when increasing Cu^{2+} and Co^{2+} concentration from 10 to 1000 μM (Fig. 5a and b), accompanied by the fluorescence color of test papers changed from purple to blue under the UV light (Fig. 5c and d). When 1 uM of Cu^{2+} and Co^{2+} was added, the fluorescence of Met-AuNC solution was largely quenched but not completely. The fluorescence color of test papers was pink which was obviously different from the orange red fluorescence color of the blank test paper, manifesting that the lowest detectable concentration of Cu^{2+} and Co^{2+} was 1 uM by the bare eyes.

Conclusions

We successfully synthesized Met-AuNCs via a facile one-step method using L-methionine as both a reducing and protecting reagent. The Met-AuNCs exhibited good properties, such as high salt stability, large Stoke's shift. Met-AuNCs were used as a fluorescent probe to determinate Cu^{2+} and Co^{2+} with a high sensitivity and selectivity. More importantly, the method had been successfully used in the detection of Cu^{2+} and Co^{2+} in real water samples. Furthermore, the Met-AuNCs based assay had been extended to test strip for the determination of Cu^{2+} and Co^{2+} with the bare eyes. The luminescent test paper also possessed satisfactory selectivity and sensitivity with a low concentration of 1 μM. The results demonstrate that the Met-AuNCs based aasay can be potentially applied in the rapid and on-site determination of Cu^{2+} and Co^{2+} in real samples.

Acknowledgments This work was funded by the Natural Science Foundation of China (NSFC) (No. 21407035), Shandong Provincial Natural Science Foundation (ZR2014BM021), Technology and Development Program of Weihai (2014DXGJ15), HIT-NSRIF (2011101).

Compliance with ethical standards The author(s) declare that they have no competing interests.

References

1. Paluch J, Mesquita RBR, Cerda V, Kozak J, Wieczorek M, Rangel AOSS (2018) Sequential injection system with in-line solid phase extraction and soil Minicolumn for determination of zinc and copper in soil leachates. Talanta 185:316–323
2. Ke B, Ma L, Kang T, He W, Gou X, Gong D, Du L, Li M (2018) In vivo bioluminescence imaging of cobalt accumulation in a mouse model. Anal Chem 90:4946–4950
3. Yao J, Zhang K, Zhu H, Ma F, Sun M, Yu H, Sun J, Wang S (2013) Efficient Ratiometric fluorescence probe based on dual-emission quantum dots hybrid for on-site determination of copper ions. Anal Chem 85:6461–6468
4. Yao Y, Tian D, Li H (2010) Cooperative binding of Bifunctionalized and click-synthesized silver nanoparticles for colorimetric Co^{2+} sensing. ACS Appl Mater Interfaces 2:684–690
5. Salnikova EV, Burtseva TI, Skalnaya MG, Skalny AV, Tinkov AA (2018) Copper and Zinc Levels in Soil, Water, Wheat, and Hair of Inhabitants of Three Areas of the Orenburg Region. Russia. Environ Res 166:158–166
6. Shoaee H, Roshdi M, Khanlarzadeh N, Beiraghi A (2012) Simultaneous Preconcentration of copper and mercury in water samples by cloud point extraction and their determination by inductively coupled plasma atomic emission spectrometry. Spectrochim Acta A 98:70–75
7. Diniz KM, Gorla FA, Ribeiro ES, Nascimento MBO, Corrêa RJ, Tarley CRT, Segatelli MG (2014) Preparation of $SiO_2/Nb_2O_5/ZnO$ mixed oxide by sol-gel method and its application for adsorption studies and on-line Preconcentration of cobalt ions from aqueous medium. Chem Eng J 239:233–241
8. Mendil D, Karatas M, Tuzen M (2015) Separation and Preconcentration of Cu(II), Pb(II), Zn(II), Fe(III) and Cr(III) ions with Coprecipitation method without carrier element and their determination in food and water samples. Food Chem 177:320–324
9. Yang FY, Jiang SJ, Sahayam AC (2014) Combined use of HPLC–ICP-MS and microwave-assisted extraction for the determination of cobalt compounds in nutritive supplements. Food Chem 147:215–219
10. Tan L, Chen Z, Zhao Y, Wei X, Li Y, Zhang C, Wei X, Hu X (2016) Dual channel sensor for detection and discrimination of heavy metal ions based on colorimetric and fluorescence response of the AuNPs-DNA conjugates. Biosens Bioelectron 85:414–421
11. Chen Y, Chen ZP, Long SY, Yu RQ (2014) Generalized Ratiometric Indicator based surface-enhanced Raman spectroscopy for the detection of Cd^{2+} in environmental water samples. Anal Chem 86: 12236–12242
12. Ding H, Liang C, Sun K, Wang H, Hiltunen JK, Chen Z, Shen J (2014) Dithiothreitol-capped fluorescent gold nanoclusters: an efficient probe for detection of Copper(II) ions in aqueous solution. Biosens Bioelectron 59:216–220
13. Sang F, Liu J, Zhang X, Pan J (2018) An aptamer-based colorimetric Pt(II) assay based on the use of gold nanoparticles and a cationic polymer. Microchim Acta 185:267
14. Duan Y, Duan R, Liu R, Guan M, Chen W, Ma J, Chen M, Du B, Zhang Q (2018) Chitosan-stabilized self-assembled fluorescent gold nanoclusters for cell imaging and biodistribution in vivo. ACS Biomater Sci Eng 4:1055–1063
15. Ishida Y, Morita A, Tokunaga T, Yonezawa T (2018) Sputter deposition toward short cationic Thiolated fluorescent gold nanoclusters: investigation of their unique structural and Photophysical characteristics using high-performance liquid chromatography. Langmuir 34:4024–4030
16. Ding C, Xu Y, Zhao Y, Zhong H, Luo X (2018) Fabrication of BSA@AuNC-based nanostructures for cell fluoresce imaging and target drug delivery. ACS Appl Mater Interfaces 10:8947–8954
17. Zheng J, Petty JT, Dickson RM (2003) High quantum yield blue emission from water-soluble Au_8 Nanodots. J Am Chem Soc 125: 7780–7781
18. Wang X, Gao W, Xu W, Xu S (2013) Fluorescent Ag nanoclusters templated by Carboxymethyl-β-Cyclodextrin (CM-β-CD) and their in vitro antimicrobial activity. Mater Sci Eng C 33:656–662
19. Zhong Y, Deng C, He Y, Ge Y, Song G (2016) Exploring a Monothiolated Beta-Cyclodextrin as the template to synthesize copper nanoclusters with exceptionally increased peroxidase-like activity. Microchim Acta 183:2823–2830
20. Halawa MI, Wu F, Fereja TH, Lou B, Xu G (2018) One-pot green synthesis of supramolecular β-Cyclodextrin functionalized gold nanoclusters and their application for highly selective and sensitive

fluorescent detection of dopamine. Sens Actuators B-Chem 254: 1017–10124

21. Zhang H, Liu Q, Wang T, Yun Z, Li G, Liu J, Jiang G (2013) Facile preparation of glutathione-stabilized gold nanoclusters for selective determination of Chromium (III) and Chromium (VI) in environmental water samples. Anal Chim Acta 770:140–146
22. Mu X, Qi L, Qiao J, Ma H (2014) One-pot synthesis of tyrosine-stabilized fluorescent gold nanoclusters and their application as turn-on sensors for Al^{3+} ions and turn-off sensors for Fe^{3+} ions. Anal Methods 6:6445–6451
23. Mu X, Qi L, Dong P, Qiao J, Hou J, Nie Z, Ma H (2013) Facile one-pot synthesis of L-proline-stabilized fluorescent gold nanoclusters and its application as sensing probes for serum iron. Biosens Bioelectron 49(15):249–255
24. Zhang Y, Hu Q, Paau MC, Xie S, Gao P, Chan W, Choi MMF (2013) Probing histidine-stabilized gold nanoclusters product by high-performance liquid chromatography and mass spectrometry. J Phys Chem C 117:18697–18708
25. Jana J, Acharyya P, Negishi Y, Pal T (2018) Evolution of silver-mediated, enhanced fluorescent Au-Ag nanoclusters under UV activation: a platform for sensing. ACS Omega 3:3463–3470
26. Jayasree M, Aparna RS, Anjana RR, Devi JSA, John N, Abha K, Manikandan A, George S (2018) Fluorescence turn on detection of bilirubin using Fe (III) modulated BSA stabilized copper nanocluster; a mechanistic perception. Anal Chim Acta 1031: 152–160
27. Shang L, Dorlich RM, Brandholt S, Schneider R, Trouillet V, Bruns M, Gerthsen D, Nienhaus GU (2011) Facile preparation of water-soluble fluorescent gold nanoclusters for cellular imaging applications. Nanoscale 3:2009–2014
28. Bian RX, Wu XT, Chai F, Li L, Zhang LY, Wang TT, Wang CG, Su ZM (2017) Facile preparation of fluorescent Au nanoclusters-based test papers for recyclable detection of Hg^{2+} and Pb^{2+}. Sens Actuators B-Chem 241:592–600
29. Wu Z, Chen J, Jin R (2011) One-pot synthesis of $Au_{25}(SG)_{18}$ 2-and 4-nm gold nanoparticles and comparison of their size-dependent properties. Adv Funct Mater 21:177–183
30. Yang JY, Yang T, Wang XY, Chen ML, Yu YL, Wang JH (2018) Mercury speciation with fluorescent gold nanocluster as a probe. Anal Chem 90:6945–6951
31. Zu F, Yan F, Bai Z, Xu J, Wang Y, Huang Y, Zhou X (2017) The quenching of the fluorescence of carbon dots: a review on mechanisms and applications. Microchim Acta 184:1899–1914
32. Liang Z, Kang M, Payne GF, Wang X, Sun RC (2016) Probing energy and Electron transfer mechanisms in fluorescence quenching of biomass carbon quantum dots. ACS Appl Mater Interfaces 8:17478–17488
33. Wang F, Hao Q, Zhang Y, Xu Y, Lei W (2016) Fluorescence Quenchometric method for determination of ferric ion using boron-doped carbon dots. Microchim Acta 183:273–279
34. Xu Y, Li H, Hu T, Su X (2017) A novel Fluorimetric sensing platform for highly sensitive detection of organophosphorus pesticides by using egg white-encapsulated gold nanoclusters. Biosens Bioelectron 91:232–237